Global and Planetary Change 82-83 (2012) 74–85

Contents lists available at SciVerse ScienceDirect

Global and Planetary Change

journal homepage: www.elsevier.com/locate/gloplacha

Comparison of modeled and geodetically-derived glacier mass balance for Tiedemann and Klinaklini glaciers, southern Coast Mountains, British Columbia, Canada

Christina Tennant [a,b,*], Brian Menounos [a,b], Bruce Ainslie [a,c], Joseph Shea [a,b,d], Peter Jackson [a,c]

[a] Natural Resources and Environmental Studies Institute, University of Northern British Columbia, Prince George, British Columbia, V2N 4Z9, Canada
[b] Geography Program, UNBC, Canada
[c] Environmental Science and Engineering Program, UNBC, Canada
[d] Department of Geography, University of British Columbia, Vancouver, BC, V6T 1Z2, Canada

ARTICLE INFO

Article history:
Received 21 July 2011
Accepted 10 November 2011
Available online 20 November 2011

Keywords:
southern Coast Mountains
glacier change
mass balance
positive-degree day model

ABSTRACT

Predicting the fate of mountain glaciers requires reliable observational data to test models of glacier mass balance. Using glacier extents and digital elevation models (DEMs) derived from aerial photographs and ASTER satellite imagery, we calculate changes in area, elevation, and volume of Tiedemann and Klinaklini glaciers. Between 1949 and 2009, Tiedemann and Klinaklini glaciers lost approximately 10% of their area. The total area-averaged thinning of Klinaklini was 40.1 ± 1.5 m water equivalent (w.e.) and total mass loss equaled 20.24 ± 1.36 km^3 w.e., whereas Tiedemann Glacier thinned by 25.7 ± 1.9 m w.e. and lost 1.69 ± 0.17 km^3 w.e. of ice. We attribute lower observed rates of thinning at Tiedemann Glacier to thick debris cover in the ablation area. Both glaciers thickened at mid-elevations after the year 2000. Glacier mass balance and volume change were modeled using temperature, precipitation and evapotranspiration fields dynamically downscaled to the mesoscale (8 km resolution) using the Regional Atmospheric Modeling System (RAMS) model and further statistically downscaled to the glacier scale (100 m elevation bands) using modeled surface lapse rates. The mass balance model over-predicts total volume loss by 1.1 and 6.3 times the geodetic loss for Klinaklini and Tiedemann glaciers respectively. Differences in modeled and observed total ice loss are due to (1) the coarse resolution of the downscaled climate fields, and (2) extensive debris cover in the ablation area of Tiedemann Glacier. Future modeling efforts should dynamically downscale at resolutions that capture the topographic complexity of a region and employ strategies to account for time-evolving debris cover.

1. Introduction

Glaciers are integral to many natural and human systems, making them important targets for monitoring and prediction. Although mountain glaciers only constitute 3–4% of global glacierized area, their recent recession significantly contributes to sea level rise (Arendt et al., 2002; Dyurgerov, 2003; Berthier et al., 2004; Larsen et al., 2007; Meier et al., 2007; Berthier et al., 2010). Mountain glaciers are the second largest contributor to recent sea-level rise (Cazenave and Nerem, 2004), and the total volume of glaciers in western Canada and Alaska has been estimated to contain a sea-level equivalence of 5 and 68 mm, respectively (Radić and Hock, 2010). Changes in glacier thickness and volume can also influence the magnitude and timing of surface runoff, affecting water supply for agriculture, consumption, and hydropower generation (Barry, 2006; Stahl and Moore, 2006; Moore et al., 2009). Given recent trends in mean global surface temperatures, and projections of continued warming, glaciers in western North America and throughout the world are expected to continue to retreat. To estimate future changes in volume and area, methods to estimate the mass balance of glaciers under a given climate scenario are required.

Glacier mass balance models to predict the fate of glaciers vary from simple ones that use accumulated air temperature anomalies (positive degree days) to those that employ a full energy balance (Braithwaite and Zhang, 1999; Casal et al., 2004; Hock and Holmgren, 2005). Positive degree day models empirically relate glacier melt and air temperature; these empirical models assume that air temperature integrates the individual fluxes of the surface energy balance. Melt factors for snow and ice have been shown to be similar among glaciers within a region (Shea et al., 2009), but can vary temporally at inter-annual to inter-decadal time scales (Huss et al., 2009; Shea et al., 2009). Temporally varying melt factors introduce uncertainty in mass balance modeling using a PDD approach, but the magnitude of this error is difficult to quantify in data-poor regions. In the current study, the lack of available input data to drive a melt model using an energy balance approach is limited by the lack of required input data. Snow accumulation is typically calculated from the total

* Corresponding author at: Natural Resources and Environmental Studies Institute, University of Northern British Columbia, Prince George, British Columbia, V2N 4Z9, Canada. Tel.: +1 250 960 5899.
E-mail address: tennant@unbc.ca (C. Tennant).

0921-8181/$ – see front matter
doi:10.1016/j.gloplacha.2011.11.004

precipitation that falls as snow, and must be melted before ice melt can occur (Braithwaite and Zhang, 1999; Shea et al., 2009).

Predicting the fate of mountain glaciers requires reliable melt modeling strategies and temporally and spatially distributed data that can be used to test these approaches. The use of remote sensing has increased the number of glaciers monitored and extended the mass balance record in regions where few traditional mass balance records exist (Berthier et al., 2004; Luthcke et al., 2008). While glacier length and area are commonly measured, changes in volume and mass balance provide a more direct, reliable indicator of climate change and can be used to verify the results of mass balance models (Kääb, 2002; Berthier et al., 2004; Barry, 2006).

The objectives of this paper are to determine change in area, elevation, and volume at Klinaklini and Tiedemann glaciers in the southern Coast Mountains British Columbia using digital elevation models (DEMs) derived from multiple sets of aerial photographs and satellite images. We expand on the results of VanLooy and Forster (2008) by incorporating DEMs that post-date the Shuttle Radar Topography Mission (SRTM), and also extend our analysis back in time to include pre-1970 data. In addition, we explore the climatic and site-specific factors that explain observed differences in area and volume change for these two glaciers. Finally, we test whether glacier mass balance estimates obtained from a hybrid modeling strategy agrees with geodetically-derived changes in glacier volume.

2. Study area

Tiedemann and Klinaklini glaciers are located in the southern Coast Mountains, approximately 300 km northwest of Vancouver, British Columbia, Canada (Fig. 1). The southern Coast Mountains are primarily influenced by moist maritime air masses, and large precipitation amounts occur as a result of orographic forcing. The winters are wet and the summers are dry with most precipitation occurring between October and March in the form of snow (Koch et al., 2009).

Both glaciers lie in close proximity to Mount Waddington, which is the highest peak in the southern Coast Mountains (4010 m above sea level — asl). Tiedemann and Klinaklini are mountain valley glaciers and, to our knowledge, do not surge. Tiedemann Glacier flows east from Mount Waddington over an elevation range of 3400 m (500–3900 m asl) and has an area of 62 km^2. Debris covers 27% of the surface area of Tiedemann Glacier, mainly in the ablation area. Klinaklini Glacier descends from the Ha-Iltzuk Icefield approximately 40 km west of Tiedemann Glacier. The glacier flows south and coalesces with the westward flowing Silverthrone Glacier some 15 km from the terminus. The total contributing ice covers an area of 480 km^2, about 56% of the Ha-Iltzuk Icefield, and ranges in elevation from about 100 to 2800 m asl. Klinaklini Glacier has little debris on its surface (3%), and it currently terminates in a proglacial lake. We collectively refer to Klinaklini and Silverthrone glaciers in this paper as Klinaklini Glacier.

3. Methods

3.1. Geomatic data

We used DEMs and glacier extents derived from aerial photographs and satellite images to determine area, volume, and elevation change of Tiedemann and Klinaklini glaciers over the past 60 years (Table 1). The National Topographic Database (NTDB) data includes glacier extents and contours derived from photographs acquired in 1970. The geometric accuracy is ±25 m in rural areas and ±125 m in isolated areas, and the contour interval is approximately 40 m (Geomatics Canada, 1996). We also used data from the Terrain Resource Information Management program (TRIM). These data include glacier extents, elevation data, and land cover, derived from 1986 aerial photographs and have a horizontal and vertical accuracy of ±10 m and ±5 m, respectively (BC Ministry of Environment, Lands and Parks, 2002). Both NTDB and TRIM data are horizontally referenced to the North American Datum of 1983 (NAD83) and vertically referenced to Mean Sea Level (Canadian Vertical Geodetic Datum, CVGD). Elevation and volume change of Tiedemann and Klinaklini glaciers for the period 1970–1986 reflect sequential DEM analysis derived from the contours and gridded elevation data.

We also extracted glacier extents and DEMs from digital scans of aerial photographs (AP) for the years 1949, 1965, 1989, 1994, and 2005, and from Advanced Spaceborne Thermal Emission and Reflection radiometer (ASTER) images for 2000, 2002, 2004, and 2006 using PCI Geomatica OrthoEngine v.10.2 (Table 1). Aerial photographs include those archived in the Canadian National Air Photo Library, the British Columbia Government, and BC Hydro. Dates of the imagery range from the end of July to the end of September. We produced a recent DEM of Tiedemann Glacier from aerial photographs taken on July 29, 2009. The acquired 1:18,000 scale color negatives were photogrammetrically scanned at a resolution of 14 μm which equates to a ground sampling distance of 0.25 m.

3.2. DEM production

The aerial photographs were co-registered in OrthoEngine v.10.2 using TRIM, 1.0 m resolution orthoimages from 2005 for Tiedemann Glacier and TRIM aerial diapositives with triangulation points (PUG points) from 1986 for Klinaklini Glacier, both referenced to NAD83

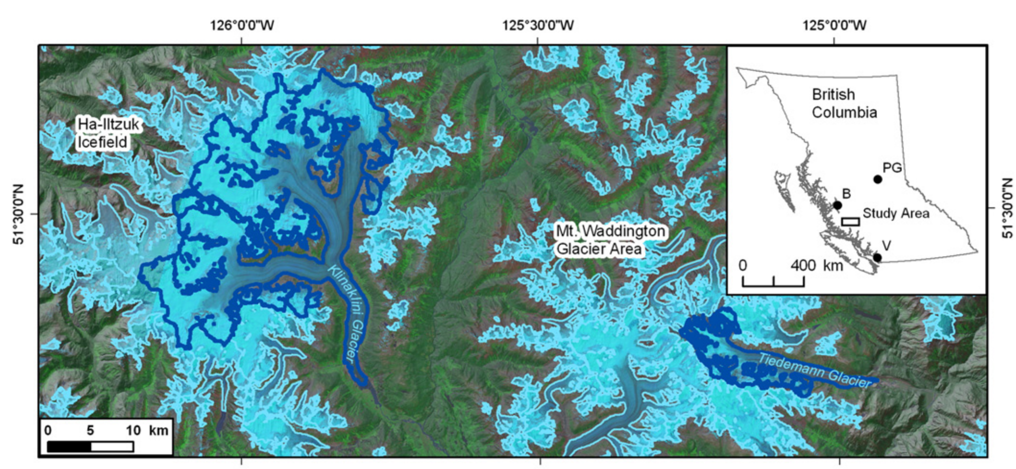

Fig. 1. Location of Klinaklini and Tiedemann glaciers in the southern Coast Mountains, British Columbia. Inset map: PG = Prince George, V = Vancouver, B = Bella Coola.

Table 1
Years of data used to extract glacier extents and digital elevation models for calculating glacier change. AP = aerial photographs, NTDB = National Topographic Database data, TRIM = Terrain Resource Information Management program, ASTER = Advanced Spaceborne Thermal Emission and Reflection radiometer.

Glacier	Data	AP	AP	NTDB	TRIM	AP	AP	ASTER	ASTER	ASTER	AP	ASTER	AP
	Year	1949	1965	1970	1986	1989	1994	2000	2002	2004	2005	2006	2009
Klinaklini	Date	8/08[a]	7/27[a]	8/30	7/26[a]	–	–	9/21	–	7/23	–	7/20	–
Tiedemann	Date	8/02[a]	7/30	8/30	7/20	8/07	7/17[a]	8/04	9/27	–	8/10[a]	–	7/29

[a] Weighted averaged date.

and Mean Sea Level. The nadir and backward-looking bands of the ASTER images were co-registered with TRIM lake vectors and mountain peaks. The 1986 TRIM DEM was used to collect elevations for ground control points (GCPs). We collected 20–30 GCPs for the aerial photographs and 30–40 GCPs for the ASTER images in accordance to Barrand et al. (2009), who found that models with greater than 20–25 GCPs produced the most accurate measurements of glacier volume change. Prominent, stable features such as bedrock outcrops, stationary boulders, or small lakes were used as GCPs and distributed at a variety of elevations surrounding the glaciers. The same GCPs were used throughout subsequent years of photography and imagery where possible to improve co-registration of DEMs (Schiefer and Gilbert, 2007) and to ensure that errors in elevation from the GCPs were randomly distributed (Krimmel, 1999). Tie points were collected to connect the images together, and a bundle adjustment using a least squares algorithm was run to rectify the images and produce an orthoimage and a DEM.

The PCI software produces DEMs using a correlation-based image-matching algorithm which matches similar patterns of pixels and determines the elevation based on parallax (Kääb, 2002; Schiefer and Gilbert, 2007). We produced DEMs with a nominal ground sampling resolution of 5 m from the aerial photographs and 15 m from the ASTER images. The analysis included the collection of correlation coefficient images with values that ranged from zero (0) to perfect correlation (100). This image was used to remove pixels with a score of less than 70, as values below this threshold were assumed to represent errors associated with poor contrast, primarily in the flat, snowy accumulation area and dark shadows (Kääb and Vollmer, 2000; Kääb, 2002; Berthier et al., 2007; Schiefer and Gilbert, 2007; Schiefer et al., 2007; VanLooy and Forster, 2008). We subsequently resampled the DEMs to 25 m to match the posting of the TRIM data.

For the 2009 air photos, we produced a DEM using the VR Mapping photogrammetry software suite. Using a similar process to that described above, we collected GCPs and tie points to create an exterior orientation file to produce stereo models. We manually collected elevation data on a 100 m grid from the 2005 and 2009 stereo models.

3.3. Glacier change

Differencing consecutive DEMs is the approach we used to determine changes in surface elevation of the glaciers. To account for areas within the accumulation area where the image matching algorithm failed due to poor photographic contrast, we determined mean elevation change for 100 m elevation bands and weighted these estimates according to the area of the band. Profiles of geodetic balance distribution over the observation period for each 100 m elevation band were also created. Some elevation bands in the accumulation area had little or no elevation points due to incomplete coverage. The area of the elevation bands with no data respectively represented approximately 0.5% and 5% for Tiedemann and Klinaklini glaciers. For elevation bands in the accumulation area with no data points, we used the average elevation change of the accumulation area as an estimate for these bands. The accumulation areas, based on average snow lines obtained from the orthoimages, lie above 1700 and 1400 m asl, respectively, for Tiedemann and Klinaklini glaciers.

For 1949 and 1965, Klinaklini Glacier had no photo coverage in the north and northwest accumulation area, but elevation points were collected in other areas at the same elevation as the missing coverage. In order to estimate total volume change, for Klinaklini in 1949 and 1965, we applied the average elevation change calculated from the elevation points within the photo coverage to the entire elevation band. Volume change was calculated by multiplying the mean elevation change of the 100 m elevation bands by the area of each band and summing the bands.

Water equivalent values were calculated per 100 m elevation band using ice densities in the accumulation and ablation areas of 550 kg m^{-3} and 900 kg m^{-3}, respectively (Schiefer et al., 2007). Based on average snow line elevation from the aerial photographs and satellite imagery, the ablation area was determined to lie below 1700 m and 1400 m for Tiedemann and Klinaklini, respectively.

For the 2005 and 2009 DEMs of Tiedemann Glacier, we calculated elevation change by differencing the elevations at each point on the 100 m grid. Volume change represents the product of this elevation change and the area of the glacier in 2005.

We also mapped glacier extents from orthoimages created during the DEM generation process. Some years of photography did not have full coverage of the accumulation area, so we were unable to map their upper elevations. We observed negligible changes in area from years of photography with full coverage of the accumulation area, however. In cases of partial coverage we thus supplemented the extents with glacier extents of the accumulation area from the TRIM data. Differencing consecutive glacier extents yielded changes in glacier area.

3.4. Error analysis

We determined an error term for the glacier extents by calculating the area of a buffer around the extents equivalent to the horizontal error of the orthoimage or data used to extract the extents (Granshaw and Fountain, 2006). Systematic error in the elevation change surface can result from the software algorithm and imperfect co-registration (Kääb and Vollmer, 2000; Kääb, 2002; Berthier et al., 2007; Schiefer and Gilbert, 2007; Schiefer et al., 2007; VanLooy and Forster, 2008). These factors can cause large errors on steep slopes and elevation bias on non-glaciated terrain. To assess the magnitude of this error term, we analyzed elevation differences in areas of stable barren terrain (i.e. no ice or vegetation) where no elevation change was expected (Fig. 2A). Most of the effects of systematic errors were removed by differencing trend surfaces from the elevation change surfaces. We also linearly modeled elevation bias remaining in the elevation change surfaces and removed it (Fig. 2B). The standard error of these non-glaciated/non-vegetated areas was assumed to represent the random error in the elevation change surfaces. We calculated this term using the standard deviation of the elevation change on the barren terrain, divided by the square root of the effective sample size (Griffith, 2005).

Adopting the approach described in VanLooy and Forster (2008), we added 5 m to the mean elevation change in each band in the

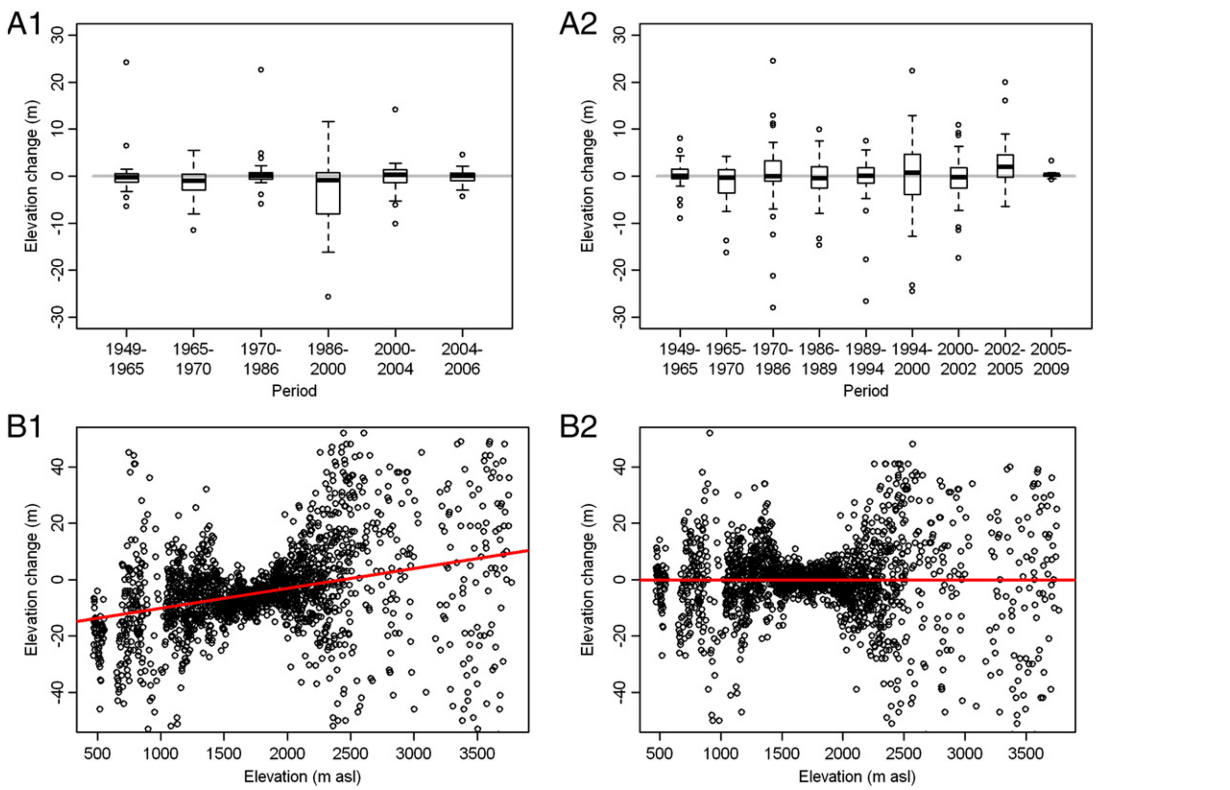

Fig. 2. Boxplots of mean elevation change of barren terrain for Klinaklini (A1) and Tiedemann (A2) glaciers. Example of elevation bias (B1) observed in the period 1986–1989 for Tiedemann Glacier and the corrected elevations (B2).

accumulation area, recalculated the volume change, and used the difference between the two volumes as an error term representing the poor image contrast in the accumulation area of the glaciers. The root mean square of the elevation change error, the area error and the uncertainty of the volume in the accumulation area represented the total error in the volume change.

3.5. Mass balance model

Glacier mass balance was modeled using a degree-day approach with downscaled meteorological fields obtained from the Regional Atmospheric Modeling System (RAMS). RAMS was first used to dynamically downscale North American Regional Reanalysis (NARR) data (Mesinger et al., 2004) from 32 km to 8 km resolution (Ainslie and Jackson, 2010). Since NARR data only extend back to 1979, we employed singular value decomposition (SVD) to downscale lower resolution ($2.5° \times 2.5°$) National Centers from Environmental Prediction (NCEP) reanalysis data (Kalnay et al., 1996) for the period 1949–2009. For the training period 1979–2004, we identified common modes of variability between the dynamically downscaled NARR output and the downscaled NCEP output. Statistical relations obtained from the training period were subsequently used to downscale NCEP fields between 1949 and 2009, giving daily temperature (T), precipitation (P), and evapotranspiration (E) fields at 8 km resolution over the study region.

For each glacier, mean daily values and surface gradients of T, P, and E were calculated from the daily climate fields using glacier masks (Fig. 3) and RAMS topography. Glacier-specific gradients were then used to estimate T, P, and E for the mid-points of 100 m elevation bands at each glacier. Gradients of precipitation and evapotranspiration were scaled by the ratio of the RAMS elevation range to the observed (TRIM), as RAMS 8 km model topography shows a much lower range in elevations over each glacier than the TRIM-based elevation range. This adjustment prevents downscaled precipitation rates falling below zero at the higher elevation bands and limits excess precipitation at the lower elevation bands.

For each elevation band and glacier, winter mass balance (b_w) was calculated as the difference total between modeled daily precipitation (P_{day}) and evapotranspiration (E_{day}) between 1 October and 14 May:

$$b_w = \Sigma\left(P_{day} - E_{day}\right). \tag{1}$$

Furthermore, in order to exclude rain events, precipitation amounts throughout the year were only considered on days where the daily average modeled temperature (T_{day}) was above 2 °C.

Accumulated positive degree days (PDD) were calculated between 15 May and 30 September. Summer glacier mass balance (b_s) is the sum of snow and ice melt (in m w.e.):

$$b_s = PDD_s \bullet k_s + PDD_i \bullet k_i \tag{2}$$

where k_s and k_i are snow and ice melt factors, respectively, and PDD_s and PDD_i are positive degree days for snow and ice melt, respectively. The values of PDD_s and PDD_i were determined by first melting the accumulated winter snow, and any remaining degree days are used to melt ice. Net mass balance is the difference between winter and summer balances.

Melt factors for snow (k_s) and ice (k_i) were determined using observed mass balance data collected from Bench, Bridge, Helm, Place, Sykora, Tiedemann, and Zavisha glaciers, all located within the southern Coast Mountains and the RAMS model domain (Mokievsky-Zubok et al., 1985; Dyurgerov, 2002). The methods used to calculate the snow and ice melt factors were similar to those used by Shea et al. (2009) with the exception that modeled RAMS air temperatures were used instead of the Stahl et al. (2006) interpolated fields. The RAMS calculated melt factors produced a better fit to the observations than the interpolated fields (RMSE of 679 mm snow water equivalent (s.w.e.) compared to

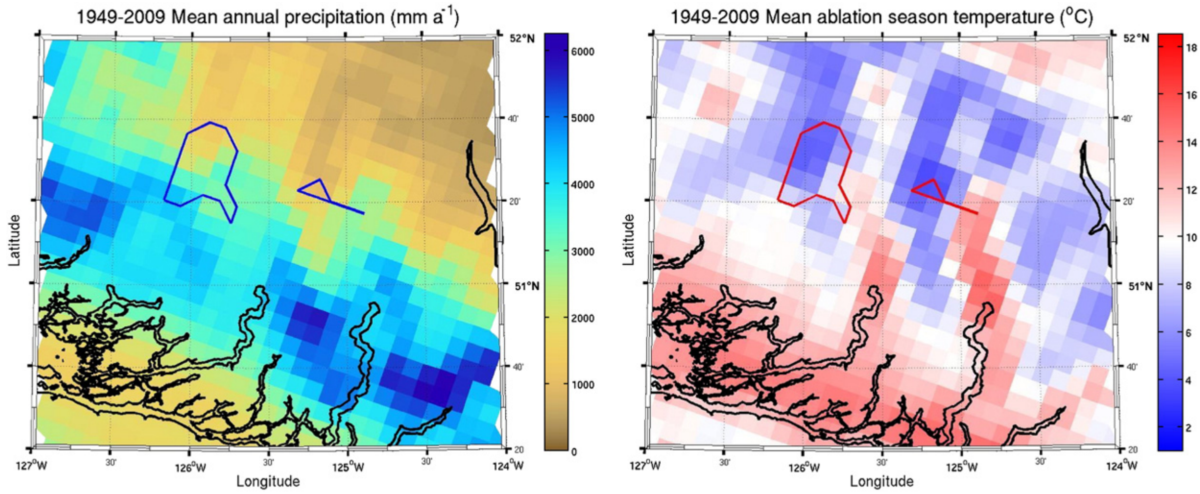

Fig. 3. Mean annual precipitation (left) and mean ablation season temperature (right) dynamically downscaled from the North American Regional Reanalysis (NARR) using the Regional Atmospheric Modeling System (RAMS). Also shown are Klinaklini and Tiedemann glaciers (blue and red lines). (For interpretation of the references to color in this figure legend, the reader is referred to the web version of this article.)

795 mm). For Tiedemann Glacier, we used melt factors derived from the observed mass balance record ($k_i = 3.55$ mm d^{-1} K^{-1} and $k_s = 2.37$ mm d^{-1} K^{-1}). For Klinaklini, where no mass balance data exist, we used melt factors averaged over the seven glaciers ($k_i = 3.83$ mm d^{-1} K^{-1} and $k_s = 3.12$ mm d^{-1} K^{-1}).

Annual volume change for each glacier between 1949 and 2009 was calculated for each elevation band as the product of modeled net mass balance and surface area. As glacier area responds to climatic changes, the use of static glacier geometry may lead to biased estimates of volume change, particularly over long timescales (Jóhannesson, 1997). This bias arises from the glacier's attempt to adjust its area-elevation distribution (hypsometry) to accommodate a new climatic regime. Under a warming climate, for example, a mass balance model using static glacier geometry may generate ice melt even though the glacier has retreated upvalley. To estimate the magnitude of this bias, we estimated the volume change using the 1949 glacier hypsometry of both glaciers, as well as updated glacier hypsometry for each period. By summing the data from each elevation band, we estimated the yearly total volume change for each glacier.

For each period, we compared the average modeled rates of volume change as well as the modeled mass balance per 100 m elevation band with the geodetic values to verify the model.

4. Results

4.1. Area change

From 1949 to 2009, Tiedemann Glacier lost an area of 5.98 ± 0.57 km^2 while Klinaklini Glacier shrank by 42.07 ± 0.29 km^2 over the period 1949 to 2006. These area changes equate to percentage and rate losses of 9.03 ± 0.60% (0.150 ± 0.010% a^{-1}) and 8.32 ± 0.05% (0.146 ± 0.001% a^{-1}) respectively for Tiedemann and Klinaklini glaciers (Table 2). Over shorter time periods, however, these rates vary between glaciers and may indicate differences in the response times of the glaciers (Fig. 4).

The terminus of Tiedemann Glacier retreated a total of 2.9 km from 1949 to 2009; between 1970 and 1994, however, the glacier advanced 0.3 km. The area of the glacier increased 1.35 ± 0.19% and

Table 2
Glacier changes of Klinaklini and Tiedemann.

Period	Δ Area (%)	Δ Area rate (% a^{-1})	Δ Elevation[a] (m w.e.)	Δ Elevation rate (m w.e. a^{-1})	Δ Volume (km^3 w.e.)	Δ Volume rate (km^3 w.e. a^{-1})
Klinaklini Glacier						
1949–1965[b]	−2.3 ± 0.01	−0.15 ± 0.001	−6.6 ± 2.4	−0.41 ± 0.15	−3.44 ± 1.71	−0.21 ± 0.11
1965–1970[b]	−1.2 ± 0.09	−0.25 ± 0.018	−2.4 ± 1.2	−0.49 ± 0.24	−1.24 ± 1.30	−0.25 ± 0.26
1970–1986	−0.5 ± 0.09	−0.03 ± 0.006	−8.8 ± 0.8	−0.55 ± 0.05	−4.44 ± 1.26	−0.28 ± 0.08
1986–2000	−3.2 ± 0.02	−0.22 ± 0.002	−22.4 ± 1.7	−1.60 ± 0.12	−11.19 ± 1.42	−0.80 ± 0.10
2000–2004	−0.6 ± 0.03	−0.14 ± 0.007	−0.4 ± 0.9	−0.10 ± 0.21	−0.20 ± 1.18	−0.05 ± 0.30
2004–2006	−0.5 ± 0.02	−0.25 ± 0.012	0.6 ± 1.1	0.28 ± 0.54	0.27 ± 1.22	0.13 ± 0.61
1949–2006	−8.3 ± 0.05	−0.15 ± 0.001	−40.1 ± 1.5	−0.70 ± 0.03	−20.24 ± 1.36	−0.36 ± 0.02
Tiedemann Glacier						
1949–1965	−1.37 ± 0.01	−0.086 ± 0.001	−8.0 ± 1.4	−0.50 ± 0.09	−0.54 ± 0.15	−0.034 ± 0.009
1965–1970	1.35 ± 0.19	0.270 ± 0.038	1.7 ± 2.5	0.35 ± 0.51	0.12 ± 0.20	0.023 ± 0.041
1970–1986	−4.78 ± 0.19	−0.299 ± 0.012	−8.5 ± 1.8	−0.53 ± 0.11	−0.58 ± 0.20	−0.036 ± 0.013
1986–1989	0.40 ± 0.03	0.134 ± 0.010	−0.7 ± 2.6	−0.24 ± 0.87	−0.05 ± 0.20	−0.015 ± 0.067
1989–1994	−0.44 ± 0.01	−0.089 ± 0.002	−2.6 ± 1.3	−0.51 ± 0.26	−0.17 ± 0.14	−0.033 ± 0.028
1994–2000	−2.41 ± 0.03	−0.402 ± 0.005	5.6 ± 2.2	0.94 ± 0.37	0.36 ± 0.18	0.061 ± 0.030
2000–2002	−1.20 ± 0.06	−0.599 ± 0.030	−7.5 ± 2.2	−3.73 ± 1.10	−0.47 ± 0.18	−0.236 ± 0.089
2002–2005	−0.57 ± 0.05	−0.188 ± 0.018	−5.6 ± 2.0	−1.85 ± 0.68	−0.35 ± 0.17	−0.116 ± 0.056
2005–2009	−0.01 ± 0.01	−0.004 ± 0.004	−0.3 ± 0.1	−0.07 ± 0.03	0.02 ± 0.01	−0.004 ± 0.002
1949–2009	−9.03 ± 0.60	−0.150 ± 0.010	−25.7 ± 1.9	−0.43 ± 0.03	−1.69 ± 0.17	−0.028 ± 0.003

Note: Values are in water equivalent based on densities, 900 kg m^{-3} and 550 kg m^{-3}, for the ablation and accumulation areas respectively.
[a] Area-averaged means.
[b] Estimated values due to missing photo coverage in parts of the accumulation area.

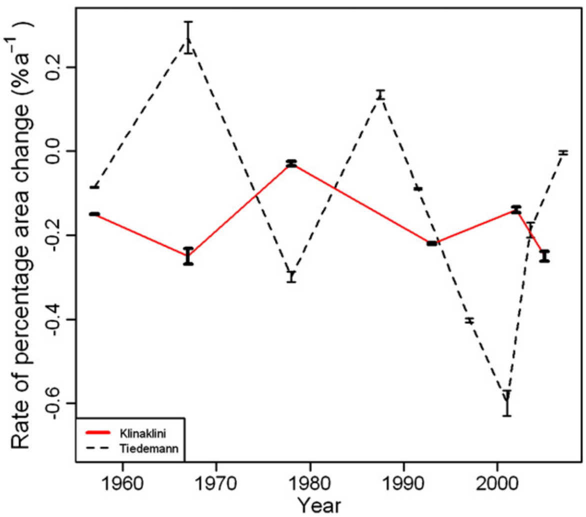

Fig. 4. Rate of percentage area change of Klinaklini (red) and Tiedemann (black, dashed) with error bars. Years are based on the midpoint of each period. (For interpretation of the references to color in this figure legend, the reader is referred to the web version of this article.)

$0.40 \pm 0.03\%$ respectively during the periods 1965–1970 and 1986–1989. These positive changes coincide with the advance of the terminus (Fig. 5). In contrast, no positive changes in either the terminus position or area occurred for Klinaklini Glacier. The terminus retreated about 3.3 km from 1949 to 2006.

4.2. Elevation change

The total area-averaged elevation change over 60 years for Tiedemann Glacier was -25.7 ± 1.9 m w.e., which corresponds to a thinning rate of -0.43 ± 0.03 m w.e. a^{-1} (Table 2). Over 57 years, Klinaklini Glacier had a total area-averaged elevation change of -40.1 ± 1.5 m w.e. and a thinning rate of -0.70 ± 0.03 m w.e.a^{-1}. Thinning rates for both glaciers vary through time (Table 2), with the highest rates shown on Klinaklini Glacier until the year 2000, after which the thinning rate for Tiedemann surpasses Klinaklini. Both glaciers experienced substantial downwasting in their ablation areas over the period of study. Total ablation area-averaged thinning for Tiedemann and Klinaklini glaciers were 80.7 ± 1.9 m w.e. and 228.2 ± 1.5 m w.e., respectively.

Klinaklini Glacier thinned most between 1986 and 2000, with an average rate of -1.60 ± 0.12 m w.e.a^{-1}, while Tiedemann's highest thinning rate was -3.73 ± 1.10 m w.e.a^{-1} during the period 2000–2002. Negligible elevation change also occurred for Tiedemann for the periods 1965–1970 and 1986–1989, and for Klinaklini following 2000 (Table 2). Some periods of observed thickening reflect

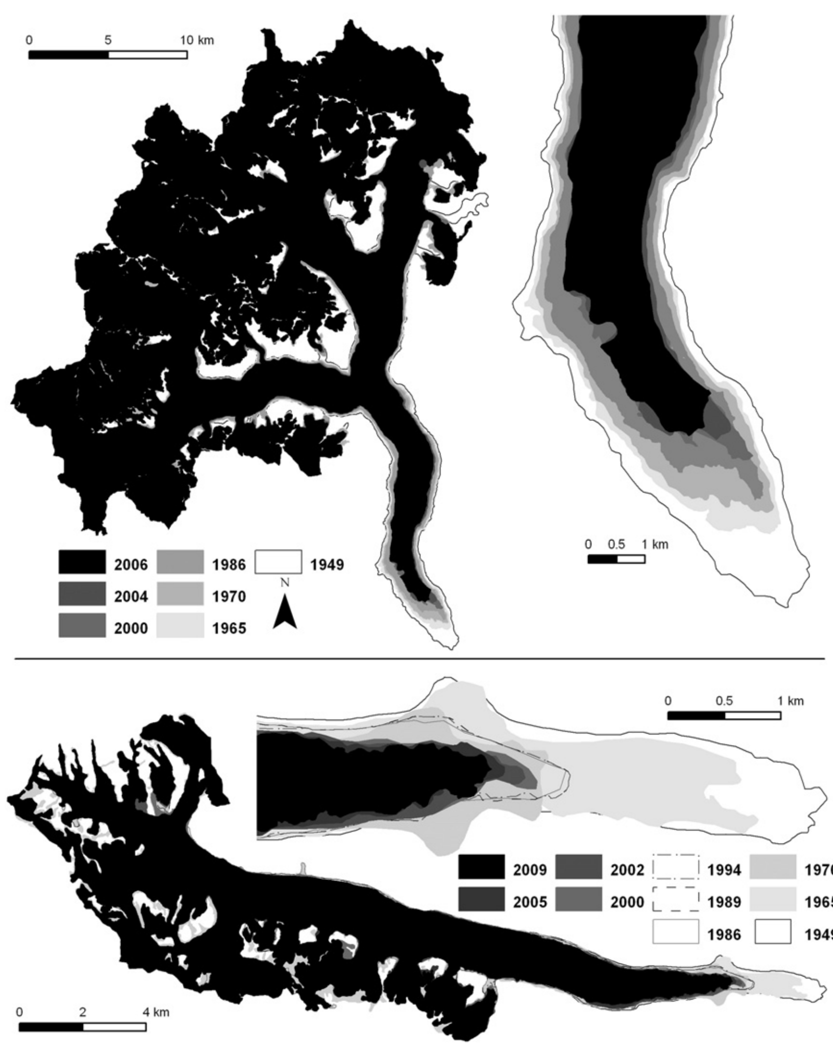

Fig. 5. Extents of Klinaklini Glacier (top) from 1949 to 2006 and Tiedemann Glacier (bottom) from 1949 to 2009.

intervals that used ASTER-derived DEMs which contain a higher uncertainty term than the DEMs based on aerial photographs (Table 2).

The spatial pattern of ice loss was similar among most periods with maximum thinning observed at the low elevations (Fig. 6). In the accumulation area, glaciers thickened by 5–10 m over some periods, but this was equal to the average error of the accumulation area for both glaciers. Maximum thinning rates up to -10 m a^{-1} occurred up glacier from the terminus, where greater thicknesses of ice were available for melt. At their margins, glaciers are thinner than along their centerlines, often leading to lower thinning rates since energy available for melt exceeds ice thickness (Berthier et al., 2010). Between 2005 and 2009, Tiedemann Glacier thickened between 1500 and 2000 m asl (Fig. 6). This thickening exceeds our calculated error term.

Profiles of geodetic balance per 100 m elevation band show notable variability through time (Fig. 7). Klinaklini Glacier experienced greatest ice loss in its ablation area, losing up to 300 m in some places over the period 1949–2009. Mass loss in the accumulation area is more variable for Tiedemann Glacier. Mass balance data measured between 1981 and 1985 at Tiedemann Glacier (Mokievsky-Zubok et al., 1985; Dyurgerov, 2002) show a similar gradient to the modeled mass balance profiles (Fig. 7). In general, geodetic balance rates are lower than either observed or modeled mass balance rates for Tiedemann Glacier.

4.3. Volume change

Tiedemann and Klinaklini glaciers respectively lost -1.69 ± 0.17 and -20.24 ± 1.36 km^3 w.e. over the period 1949–2009 (Table 2). These volume losses yield annual rates of -0.028 ± 0.003 and -0.355 ± 0.023 km^3 w.e. a^{-1}. Cumulative geodetic balances are -25.7 ± 2.6 and -40.1 ± 2.7 m w.e. for Tiedemann and Klinaklini, respectively. The glaciers had similar balances until 1986 after which Klinaklini's balance became considerably more negative over the period 1986–2000 (Fig. 8). The volume of both glaciers slightly increased in the first years of the 21st century, but this increase is only marginally greater than the error term for Tiedemann Glacier (Table 2). Large uncertainties for the ASTER DEMs preclude an assessment of whether other times of observed volume increase for the glaciers are real.

4.4. Modeled mass balance and volume change

Estimated volume change for Tiedemann and Klinaklini glaciers based on the PDD model driven with RAMS meteorological fields differ from geodetic changes (Fig. 9). Explained variance (r^2) between modeled and geodetic volume loss is 0.19 and 0.14 for Klinaklini and Tiedemann respectively. Cumulative modeled volume losses exceed the observed geodetic losses by a factor of 1.1 for Klinaklini

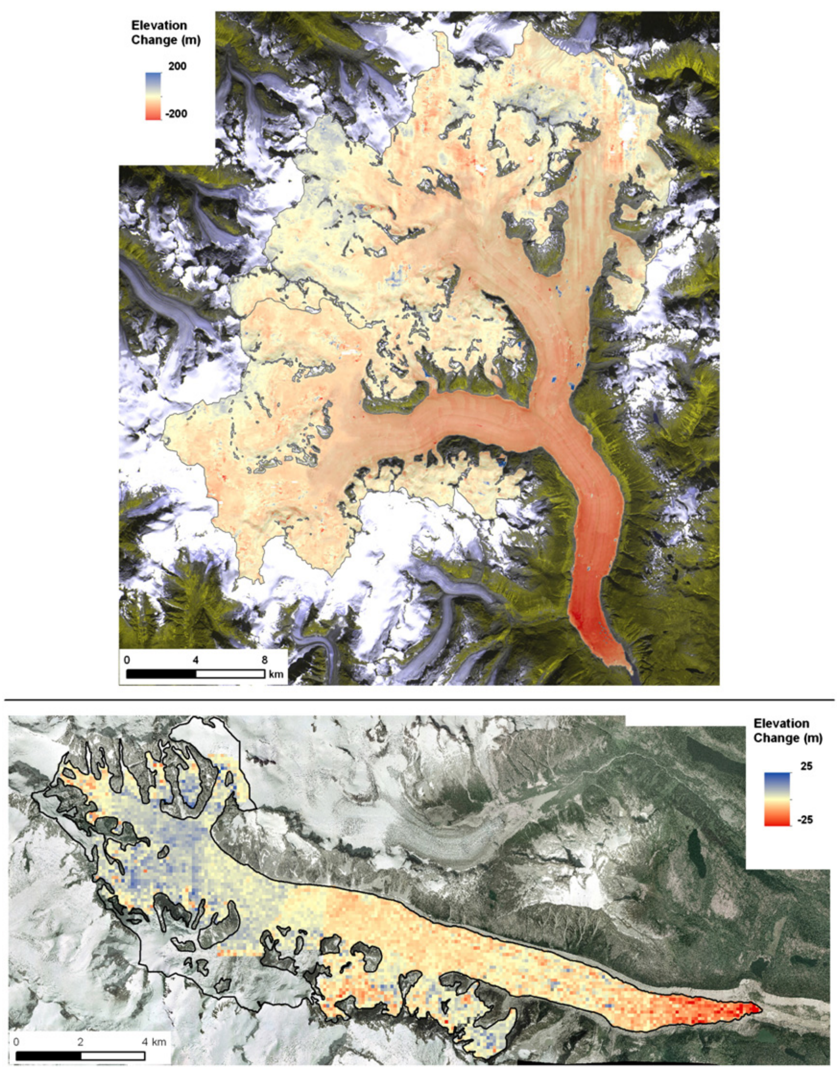

Fig. 6. Examples of elevation change surfaces for Klinaklini (top) from the period 1986–2000 (2004 Landsat5, 7-4-2 composite) and Tiedemann (bottom) from the period 2005–2009 (2005 orthoimage). (For interpretation of the references to color in this figure legend, the reader is referred to the web version of this article.)

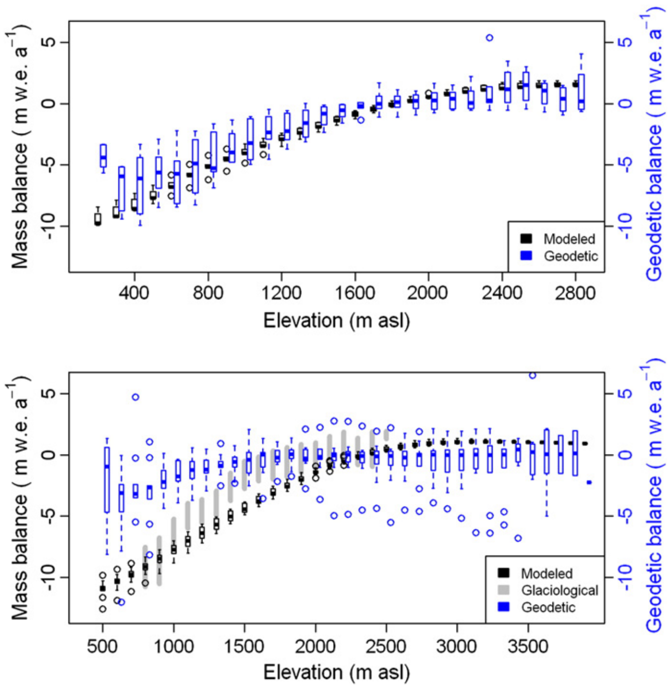

Fig. 7. Average annual modeled (black) mass balance and geodetic (blue) balance profiles per 100 m elevation band from 1949 to 2006 for Klinaklini Glacier (top) and from 1949 to 2009 for Tiedemann Glacier (bottom). The range of glaciological mass balance data collected at Tiedemann from 1981 to 1985 is also shown (gray) (Mokievsky-Zubok et al., 1985; Dyurgerov, 2002). (For interpretation of the references to color in this figure legend, the reader is referred to the web version of this article.)

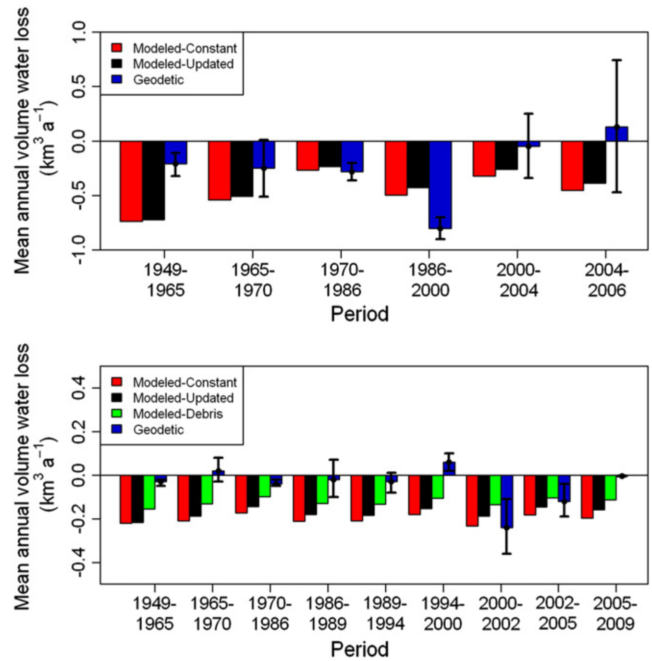

Fig. 9. Modeled volume loss with constant (red) and updated (black) area-elevation distributions, and geodetic (blue) volume loss for Klinaklini (top) and Tiedemann (bottom) glaciers. Modeled volume loss incorporating debris cover is also shown (green). (For interpretation of the references to color in this figure legend, the reader is referred to the web version of this article.)

and 6.3 for Tiedemann. We found that modeled equilibrium line altitudes (ELA) were often 300–500 m higher than the snowline altitudes observed in the imagery. At both glaciers, modeled volume loss throughout the observation period was consistently negative. The modeled volume loss of Klinaklini Glacier decreased from 1949–1965 through to 1970–1986, and accelerated between 2004 and 2006. This pattern is opposite to the observed pattern revealed in the geodetic volume loss data (Fig. 9). For Tiedemann Glacier, the modeled volume loss is less variable among periods. The mass balance model output indicates an increase in the volume loss in the first decade of the 21st century for Klinaklini and a decrease in volume loss for Tiedemann.

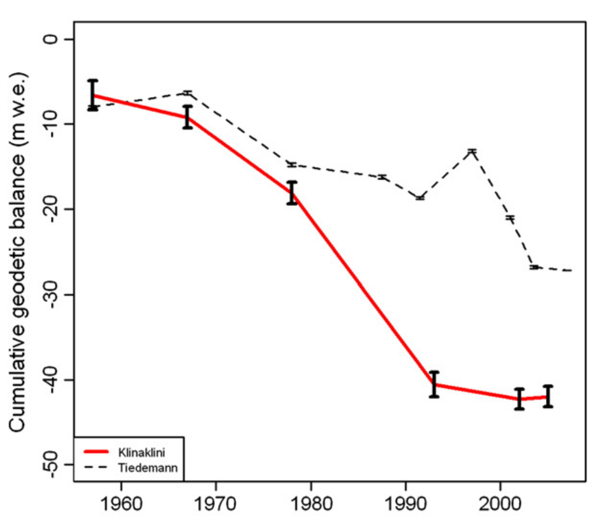

Fig. 8. Cumulative geodetic balance of Klinaklini (red) and Tiedemann (black, dashed) glaciers. Geodetic balance was calculated by dividing volume (w.e.) by glacier area. (For interpretation of the references to color in this figure legend, the reader is referred to the web version of this article.)

The constant area-elevation distribution of the 1949 glacier surface used in the model resulted in 110–120% more ice loss than using updated area-elevation distributions for the glaciers. This result indicates the potential magnitude of the bias when using a mass balance model with static glacier geometry to forecast future volume change.

Despite the discrepancies between the modeled and geodetic total volume loss, the modeled mass balance profiles (Fig. 7) were similar to the geodetic balance profiles of Klinaklini Glacier. For Tiedemann Glacier, the model consistently overestimated melt in the ablation area, but produced similar values to the glaciological mass balance data collected between 1981 and 1985 (Fig. 7).

4.5. Effect of debris cover

We do not have in-situ measurements of surface debris for Tiedemann Glacier to calculate the reduction in melt factors as a function of debris thickness. To estimate the effect of debris cover on the modeled mass balance, we arbitrarily scale the original ice melt factor for Tiedemann ($k_i = 3.55$ mm K^{-1} d^{-1}) by as much as 50% based on the percentage of debris cover (PDC) for a given elevation band z:

$$k_{i(z)} = k_i - 0.5\left(k_i \bullet PDC_{(z)}/100\right) \quad (3)$$

which yields ice melt factors ranging from 1.8 mm K^{-1} d^{-1} (100% debris cover) to 3.55 mm K^{-1} d^{-1} (0% debris cover). This scaling is arbitrary but conservative since negligible melt rates might be expected under 100% debris cover if its thickness exceeds 1–2 m (Kayastha et al., 2000). Incorporating debris-cover in the model in this manner reduced the discrepancy between modeled and geodetic cumulative

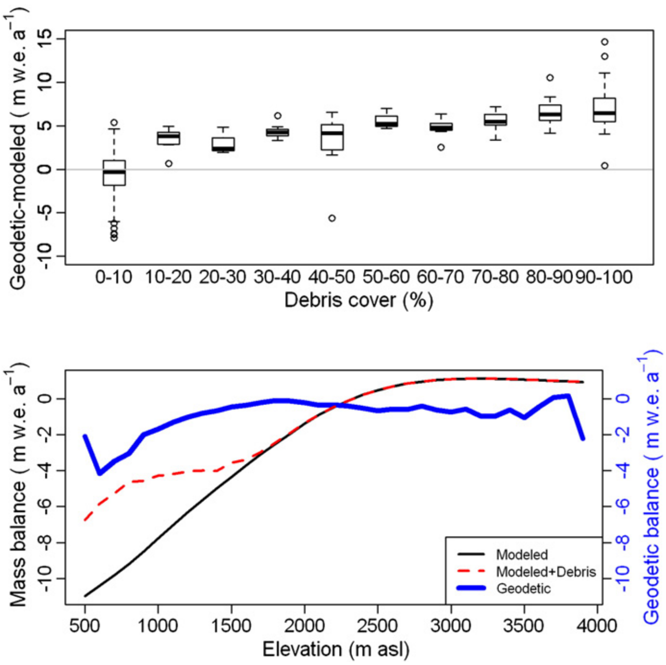

Fig. 10. Differences between the modeled and geodetic balance by percent debris cover (top) for Tiedemann Glacier. Mass balance incorporating debris cover was modeled by scaling the melt factor to percent debris cover. Modeled mass balance profiles with (red, dashed) and without (black) debris cover and the geodetic balance (blue) for Tiedemann Glacier (bottom). (For interpretation of the references to color in this figure legend, the reader is referred to the web version of this article.)

volume losses from a factor of 6.3 to 4.4 (Fig. 9). The profile of modeled mass balance with a debris-cover factor also shows a reduction of ice loss in the ablation area, although it is still several times greater than the geodetic loss (Fig. 10).

4.6. Early twenty first century climate

To evaluate the climatological factors that could account for the observed thickening on Tiedemann Glacier (Fig. 6), we obtained fields of mean ablation season (May–September) temperature and mean accumulation season (October–April) precipitation fields for the periods 1986–2000 and 2000–2009 from NARR (Mesinger et al., 2006). Differences in the mean fields of temperature and precipitation (Fig. 11) reveal a distinct increase in winter precipitation rates and a slight decrease in ablation season temperatures in the vicinity both glaciers.

5. Discussion

5.1. Glacier comparison

The areas of Klinaklini and Tiedemann glaciers decreased by ~10% between 1949 and 2006/2009. The pattern of thinning through time was also similar, in that the glaciers reached a peak thinning rate at the turn of the century followed by a reduction in the thinning rate, or increased thickening in Tiedemann's case. Our results suggest that regional climate variability is responsible for observed long-term dimensional changes of both glaciers. Short-term differences between the glaciers, such as the timing and magnitude of the dimensional changes, can be attributed to differing response times influenced by size, slope, and elevation range (Pelto and Hedlund, 2001), as well as other physical properties such as debris cover (Benn and Lehmkuhl, 2000).

The terminus of Tiedemann is heavily debris-covered and is situated approximately 400 m higher in elevation than the terminus of Klinaklini. We thus expected Tiedemann to shrink and thin more slowly than Klinaklini, but this was not always reflected in the area-averaged data (Table 2). The smaller glaciers that feed Tiedemann Glacier along its southern edge may have contributed to an increased thinning rate calculated at higher elevations, as well as an increased area change. Klinaklini's large accumulation area with little elevation change may have also reduced the area-averaged thinning rates (VanLooy and Forster, 2008).

For the ablation area only, elevation change rates between 1949 and 2009 for Tiedemann Glacier varied between 0.56 and -4.80 m w.e. a^{-1}, versus ablation area elevation change rates of -2.45 to -6.98 m w.e. a^{-1} for Klinaklini. Some of these differences are undoubtedly due to the insulating effects of debris cover on Tiedemann Glacier, which indicates that a consideration of glacier surface properties is important when comparing glacier changes within a region. Differences in ablation area surface elevation may also contribute to the observed differences, as the terminus at Klinaklini is located 400 m below the terminus at Tiedemann.

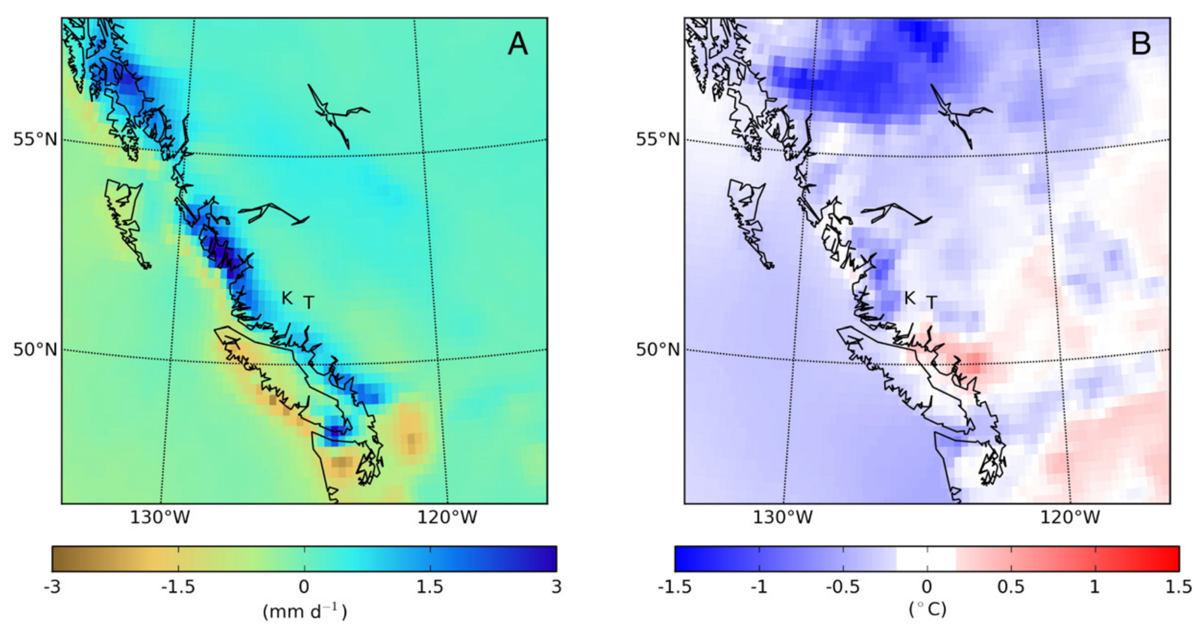

Fig. 11. Difference in NARR precipitation (A) and temperature (B) fields between 2000–2009 and 1986–2000. Location of Klinaklini (K) and Tiedemann (T) glaciers are indicated. (For interpretation of the references to color in this figure legend, the reader is referred to the web version of this article.)

5.2. Regional comparison

VanLooy and Forster (2008) calculated an area loss of -13.8 km^2 for the Ha-Iltzuk Icefield from mid-1980s to 1999, mostly from Klinaklini Glacier, comparable to our estimate from Klinaklini of -15.8 ± 0.4 km^2 over the period 1986–2000. Our rate of area-averaged elevation change from 1986 to 1999/2000 for Klinaklini (-1.60 ± 0.10 m a^{-1}) was greater than their rate for Ha-Iltzuk Icefield (-1.0 m a^{-1}), while our rate for Tiedemann (0.06 ± 0.56 m a^{-1}) was less than their rate for Mount Waddington glacier area (-0.2 m a^{-1}), but within the error term.

The behavior of Tiedemann and Klinaklini glaciers mirrors the general pattern observed for other glaciers in the southern Coast Mountains and western North America. In Garibaldi Park, British Columbia, 250 km southeast of the study area, glaciers receded rapidly between the 1920s and 1950s, advanced between 1960 and 1980, and subsequently retreated (Koch et al., 2009). In the North Cascades, Washington, USA, glaciers rapidly retreated from 1890 to 1950, slowed their retreat or advanced between 1950 and 1976, and retreated thereafter (McCabe and Fountain, 1995; Pelto, 2006). Retreat of Tiedemann and Klinaklini glaciers slowed after the mid-1960s, and the terminus of Tiedemann Glacier underwent a post-1970 advance. Collectively, these changes broadly mirror decadal scale changes in climate (Koch et al., 2009; Moore et al., 2009). Observed periods of retreat during the 1920–1940s and 1980–2000s reflected warm, dry conditions, while periods of advance or slowed retreat reflected cooler, wetter conditions during the 1950–1970s (McCabe and Fountain, 1995; Pelto, 2006; VanLooy and Forster, 2008; Koch et al., 2009).

For the southern Coast Mountains, Schiefer et al. (2007) calculated a thinning rate of -0.89 ± 0.23 m a^{-1} from 1985 to 1999 which is comparable to our average rate for Klinaklini and Tiedemann of -0.83 ± 0.34 m a^{-1} from 1986 to 2000. They also note strong negative mass balance regimes in the late 20th century. Pelto (2006) recorded a mean annual balance of -0.41 m (no error term reported) from 1984 to 2004 and a mean cumulative mass balance loss of -8.5 m w.e. for North Cascade glaciers. Differences in regional climate, elevation of ablation areas, or measurement errors may account for the observed differences in cumulative balances between glaciers in the southern Coast Mountains and the North Cascades. Nevertheless, total area loss was 7% for the North Cascades National Park Complex from 1958 to 1998 (Granshaw and Fountain, 2006), which is comparable to our 7.2% from 1949 to 2000.

In Alaska, Gulkana and Wolverine glaciers (Van Beusekom et al., 2010) thinned since the mid-1960s, but the pattern of mass change differs somewhat from the glaciers of this study. An inverse relation between mass balances of Alaskan and Washington glaciers is known (Hodge et al., 1998), and may be the cause of the difference with Klinaklini and Tiedemann which share a similar climate regime to the Washington glaciers.

From 2000 to 2009, thinning and volume loss decreased at both Klinaklini and Tiedemann glaciers. These changes mirror the mass balance record of Lemon Creek Glacier, Alaska (WGMS, 2008). The recent mid-elevation thickening at Tiedemann Glacier appears to be a response to the increase in winter precipitation rates and decrease in ablation season temperatures observed in the southern Coast Mountains (Figs. 6 and 11). Winter precipitation anomalies have been strongly linked with changes in mass balance of other maritime glaciers in western North America (McCabe and Fountain, 1995; Bitz and Battisti, 1999). Work is in progress to evaluate whether this thickening is detectable throughout the Coast Mountains.

5.3. Observed discrepancies between geodetic and modeled volume losses

A number of factors may explain the divergence between the geodetic and modeled mass balance for the glaciers of this study. Below, we discuss these factors in order of their perceived importance.

Differences between geodetic and modeled volume change reveal the importance of spatial resolution in climate downscaling. The downscaling approach and resolution used here to generate meteorological fields appear suitable for basin-scale applications (Ainslie and Jackson, 2010), but apparently cannot resolve the topographic complexity required to model mass balance for even large individual glaciers such as those of this study. In particular, the 8 km resolution of RAMS will result in a greatly smoothed topography, which will affect the timing and location of orographic and frontal precipitation in high-relief mountain terrain. The significance of topographic smoothing in biasing mass balance modeling is revealed in this study (c.f. Fig. 3) where annual precipitation maxima do not occur over the highest elevation of southern Coast Mountains, but westward over the topographic highs of the RAMS model. The westward location of these maxima also causes negative elevational precipitation gradients over both glaciers, an unrealistic situation for mountains in most maritime environments. It is clear that alternative downscaling strategies such as using mesoscale weather models at higher resolution (1 km or less) or using methods that produce precipitation fields at high spatial resolution (Jarosch et al., 2010) are required for mass balance modeling in mountains as topographically complex as those of this study.

At both sites, differences between modeled mass balance and geodetic balance were greatest in the ablation area. These differences are related to the assumption of a static ice volume, and debris cover. At the lowest elevation band of both glaciers (Fig. 7), geodetic balances are less negative than subsequent elevation bands, as the energy for melting ice at the lowest elevations is greater than the amount of ice available to melt. The presence of substantial debris cover on Tiedemann would also contribute to the overestimation of melt (Figs. 7, 9 and 10). Previous research on debris-covered glaciers has demonstrated that the presence of debris cover substantially reduces melt factors (Kayastha et al., 2000; Mihalcea et al., 2006). Landsat imagery can be used to identify debris-covered ice and reduce estimated surface albedo for mass balance models (Paul and Kotlarski, 2010). However, such maps are only valid for one to several years and data on debris thickness is still needed for determining actual melt factors on the glacier. Given the importance of debris cover on melt modeling, our attempts to quantify the change in ice melt factor based on percent degree cover represent an important first step, though more work is needed to quantify the thickness and spatial extent of surface debris and, importantly, how it varies in time.

Another factor influencing the discrepancies between the modeled and geodetic volume loss may be the derivation of the melt factors. The melt factors for Klinaklini glacier were derived from the average melt factors of glaciers in the region, whereas the melt factors for Tiedemann were derived from mass balance data recorded between 1981 and 1985. The balance profiles showed that the direct mass balance measurements also had greater melt than the geodetic measurements (Fig. 7). The difference probably arises from the averaging effects in the geodetic measurements, sampling strategies of the direct mass balance measurements, and ice dynamics. Sites for ablation stakes are those that preclude extensive debris cover and would thus overestimate surface melt for debris-rich zones.

Using updated areas of the glaciers by elevation band decreased the modeled volume changes compared to the use of constant areas, but this factor alone cannot account for differences between the geodetic and predicted mass change for the glaciers. Other factors that may account for discrepancies between modeled and observed ice loss include density estimation of snow and firn, and ice dynamics at seasonal to inter-annual time scales. Our density estimates are not based on in-situ measurements and thus, estimating an error term is difficult. Effects of seasonal dynamics (submergence, emergence) could bias our results by introducing aliasing into our data. However, this effect is believed to be minor since our modeled periods of mass change align with the acquisition date of the imagery, and separation times between much of our geodetic data is on the order of a decade. Seasonal and inter-annual to inter-decadal ice dynamics would greatly affect our analysis if our geodetic data was acquired every 1–2 years, not aligned with the modeled mass balance data (or did not model melt for those years where the imagery did not reflect the end of ablation season), or only represented the ablation areas of the glaciers. In short, we believe that errors inherent in the low-resolution dynamical downscaling and the lack of data about debris thickness explain the majority of the discrepancy between observed and modeled mass change for the glaciers of our study.

6. Conclusions

We used aerial photographs, ASTER imagery, and digital elevation data to estimate area, elevation and volume changes of Klinaklini and Tiedemann glaciers from 1949 to 2009. Over this period, both glaciers lost approximately 10% of their area. While Klinaklini consistently shrank, Tiedemann advanced 300 m in the 1970s. Klinaklini Glacier's thinning rates accelerated between 1986 and 2000, and the glacier lost a total volume of $20.24 \pm 1.36\ \mathrm{km}^3$ w.e. during the period 1946–2006. Tiedemann Glacier's thinning rates were more variable. Over the period 1949 and 2009, the glacier lost $1.69 \pm 0.17\ \mathrm{km}^3$ w.e., but thickened in its mid elevations during the period 2005–2009.

Observed geodetic changes were compared with modeled glacier mass balance derived from dynamically and statistically downscaled fields of temperature and precipitation and a PDD mass balance model. Differences between observed and modeled glacier changes are due primarily to the 8 km resolution of the numerical weather model run, the treatment of debris cover within the mass balance model, and the estimated degree day melt factors. In western North America and elsewhere, future research should focus on the development of mass balance models that incorporate surface debris, and employ dynamic downscaling at spatial resolutions that are sufficient to resolve the topographic complexity of the study domain.

Acknowledgments

We would like to thank BC Hydro for access to digital aerial photographs from 1989. Tyler Sylvestre and Caillin Smith scanned aerial photographs from the National Air Photo Library and the BC Photo Library, respectively. Cardinal Systems, LLC provided licensing and support for their VR Mapping photogrammetry software. The Natural Sciences and Engineering Research Council of Canada and the Canadian Foundation for Climate and Atmospheric Sciences (Western Canadian Cryospheric Network) funded our research. Imagery for this project was provided by the Province of British Columbia, Natural Resources Canada, and the Global Land Ice Monitoring Program from Space (GLIMS). Finally, we would also like to acknowledge the referees and editor for their careful, constructive reviews which strengthened the paper.

References

Ainslie, B., Jackson, P.L., 2010. Downscaling and bias correcting a cold season precipitation climatology over coastal southern British Columbia using the Regional Atmospheric Modeling System (RAMS). Journal of Applied Meteorology and Climatology 49 (5), 937–953.

Arendt, A.A., Echelmeyer, K.A., Harrison, W.D., Lingle, C.S., Valentine, V.B., 2002. Rapid wastage of Alaska glaciers and their contribution to rising sea level. Science 297, 382–386.

Barrand, N.E., Murray, T., James, T.D., Barr, S.T., Mills, J.P., 2009. Optimizing photogrammetric DEMs for glacier volume change assessment using laser-scanning derived ground-control points. Journal of Glaciology 55, 106–116.

Barry, R.G., 2006. The status of research on glaciers and global glacier recession: a review. Progress in Physical Geography 30, 285–306.

BC Ministry of Environment, Lands and Parks, 2002. British Columbia Specifications and Guidelines for Geomatics, Release 2.0. Victoria, British Columbia.

Benn, D.I., Lehmkuhl, F., 2000. Mass balance and equilibrium-line altitudes of glaciers in high-mountain environments. Quaternary International 65–66, 15–29.

Berthier, E., Arnaud, Y., Baratoux, D., Vincent, C., Remy, F., 2004. Recent rapid thinning of the "Mer de Glace" glacier derived from satellite optical images. Geophysical Research Letters 31, L17401. doi:10.1029/2004GL020706.

Berthier, E., Arnaud, Y., Kumar, R., Ahmad, S., Wagnon, P., Chevallier, P., 2007. Remote sensing estimates of glacier mass balances in the Himachal Pradesh (Western Himalaya, India). Remote Sensing of Environment 108, 327–338.

Berthier, E., Schiefer, E., Clarke, G.K.C., Menounos, B., Remy, F., 2010. Contribution of Alaskan glaciers to sea-level rise derived from satellite imagery. Nature Geoscience 3, 92–95. doi:10.1038/NGEO737.

Bitz, C.M., Battisti, D.S., 1999. Interannual to decadal variability in climate and the glacier mass balance in Washington, Western Canada, and Alaska. Journal of Climate 12, 3181–3196.

Braithwaite, R.J., Zhang, Y., 1999. Modelling changes in glacier mass balance that may occur as a result of climate changes. Geografiska Annaler 81A (4), 489–496.

Casal, T.G.D., Kutzbach, J.E., Thompson, L.G., 2004. Present and past ice-sheet mass balance simulations for Greenland and the Tibetan Plateau. Climate Dynamics 23 (3–4), 407–425.

Cazenave, A., Nerem, R.S., 2004. Present-day sea level change: observations and causes. Reviews of Geophysics 42, RG3001. doi:10.1029/2003RG000139.

Dyurgerov, M.B., 2002. Glacier mass balance and regime: data of measurements and analysis. Institute of Arctic and Alpine Research, Occasional Paper 55. University of Colorado, Boulder, CO.

Dyurgerov, M.B., 2003. Mountain and subpolar glaciers show an increase in sensitivity to climate warming and intensification of the water cycle. Journal of Hydrology 282, 164–176.

Geomatics Canada, 1996. Standards and Specifications of the National Topographic Data Base, Edition 3.1. Natural Resources Canada, Sherbrooke, Quebec, Canada.

Granshaw, F.D., Fountain, A.G., 2006. Glacier change (1958–1998) in the North Cascades National Park Complex, Washington, USA. Journal of Glaciology 52 (177), 251–256.

Griffith, D.A., 2005. Effective geographic sample size in the presence of spatial autocorrelation. Annals of the Association of American Geographers 95 (4), 740–760.

Hock, R., Holmgren, B., 2005. A distributed surface energy-balance model for complex topography and its application to Storglaciären, Sweden. Journal of Glaciology 51, 25–36.

Hodge, S.M., Trabant, D.C., Krimmel, R.M., Heinrichs, T.A., March, R.S., Josberger, E.G., 1998. Climate variations and changes in mass of three glaciers in Western North America. Journal of Climate 11, 2161–2179.

Huss, M., Funk, M., Ohmura, A., 2009. Strong Alpine glacier melt in the 1940s due to enhanced solar radiation. Geophysical Research Letters 36, L23501. doi:10.1029/2009GL040789.

Jarosch, A., Anslow, F., Clarke, G.K.C., 2010. High-resolution precipitation and temperature downscaling for glacier models. Climate Dynamics. doi:10.1007/s00382-010-0949-1.

Jóhannesson, T., 1997. The response of two Icelandic glaciers to climatic warming computed with a degree-day glacier mass balance model coupled to a dynamic glacier model. J. Glaciology 43 (144), 321–327.

Kääb, A., 2002. Monitoring high-mountain terrain deformation from repeated air- and spaceborne optical data: examples using digital aerial imagery and ASTER data. ISPRS Journal of Photogrammetry and Remote Sensing 27, 39–52.

Kääb, A., Vollmer, M., 2000. Surface geometry, thickness changes and flow fields on creeping mountain permafrost: automatic extraction by digital image analysis. Permafrost and Periglacial Processes 11, 315–326.

Kalnay, E., Kanamitsu, M., Kistler, R., Colins, W., Deaven, D., Gandin, L., Iredell, M., Saha, S., White, G., Woollen, J., Zhu, Y., Chelliah, M., Ebisuzaki, W., Higgins, W., Janowiak, J., Mo, K.C., Ropelewski, C., Wang, J., Leetmaa, A., Reynolds, R., Jenne, R., Joseph, D., 1996. The NCEP/NCAR 40-year reanalysis project. Bulletin of the American Meteorological Society 77 (3), 437–471.

Kayastha, R.B., Takeuchi, Y., Nakawo, M., Ageta, Y., 2000. Practical Prediction of Ice Melting beneath Various Thickness of Debris Cover on Khumbu Glacier, Nepal, Using a Positive Degree-day Factor, No. 264. IAHS Publication, pp. 71–82.

Koch, J., Menounos, B., Clague, J.J., 2009. Glacier change in Garibaldi Provincial Park, southern Coast Mountains, British Columbia, since the Little Ice Age. Global and Planetary Change 66, 161–178.

Krimmel, R.M., 1999. Analysis of difference between direct and geodetic mass balance measurements at South Cascade Glacier, Washington. Geografiska Annaler 81A, 653–658.

Larsen, C.F., Motyka, R.J., Arendt, A.A., Echelmeyer, K.A., 2007. Glacier changes in southeast Alaska and northwest British Columbia and contribution to sea level rise. Journal of Geophysical Research 112, F01007. doi:10.1029/2006JF000586.

Luthcke, S.B., Arendt, A.A., Rowlands, D.D., McCarthy, J.J., Larsen, C.F., 2008. Recent glacier mass changes in the Gulf of Alaska region from GRACE mascon solutions. Journal of Glaciology 54 (188), 767–777.

McCabe Jr., G.J., Fountain, A.G., 1995. Relations between atmospheric circulation and mass balance of South Cascade Glacier, Washington, U.S.A. Arctic and Alpine Research 27 (3), 226–233.

Meier, M.F., Dyurgerov, M.B., Ursula, R.K., O'Neel, S., Pfeffer, W.T., Anderson, R.S., Anderson, S.P., Glazovsky, A.F., 2007. Glaciers dominate eustatic sea-level rise in the 21st century. Science 317, 1064–1067.

Mesinger, F., DiMego, G., Kalnay, E., Mitchell, K., Shafran, P.C., Ebisuzaki, W., Jovic, D., Woollen, J., Rogers, E., Berbery, E.H., Ek, M.B., Fan, Y., Grumbine, R., Higgins, W., Li, H., Lin, Y., Manikin, G., Parrish, D., Shi, W., 2004. North American Regional Reanalysis: a long-term, consistent, high-resolution climate dataset for the North American domain, as a major improvement upon the earlier global reanalysis datasets in both resolution and accuracy. Submitted to the Bulletin of the American Meteorological Society, pp. 1–42.

Mesinger, F., DiMego, G., Kalnay, E., Mitchell, K., Shafran, P.C., Ebisuzaki, W., Jovic, D., Woollen, J., Rogers, E., Berbery, E.H., Ek, M.B., Fan, Y., Grumbine, R., Higgins, W., Li, H., Lin, Y., Manikin, G., Parrish, D., Shi, W., 2006. North American Regional Reanalysis. Bulletin of the American Meteorological Society 87 (3), 343–360.

Mihalcea, C., Mayer, C., Diolaiuti, G., Smiraglia, C., Tartari, G., 2006. Ablation conditions on the debris covered part of Baltoro Glacier, Karakoram. Annals of Glaciology 43, 292–300.

Mokievsky-Zubok, O., Ommanney, C.S.L., Power, J., 1985. NHRI glacier mass balance, 1964–1984 (Cordillera and Arctic). Internal Report, Environment Canada. National Hydrology Research Institute, Ottawa, Ontario.

Moore, R.D., Fleming, S.W., Menounos, B., Wheate, R., Fountain, A.G., Stahl, K., Holm, K., Jakob, M., 2009. Glacier change in western North America: influences on hydrology, geomorphic hazards and water quality. Hydrological Processes 23, 42–61.

Paul, F., Kotlarski, S., 2010. Forcing a distributed mass balance model with the regional climate model REMO, Part II: downscaling strategy and first results. Journal of Climate 23, 1607–1620.

Pelto, M.S., 2006. The current disequilibrium of North Cascade glaciers. Hydrological Processes 20, 769–779.

Pelto, M.S., Hedlund, C., 2001. The terminus behavior and response time of North Cascade glaciers. Journal of Glaciology 47, 497–506.

Radić, V., Hock, R., 2010. Regional and global volumes of glaciers derived from statistical upscaling of glacier inventory data. Journal of Geophysical Research 115, F01010. doi:10.1029/2009JF001373.

Schiefer, E., Gilbert, R., 2007. Reconstructing morphometric change in a proglacial landscape using historical aerial photography and automated DEM generation. Geomorphology 88, 167–178.

Schiefer, E., Menounos, B., Wheate, R., 2007. Recent volume loss of British Columbian glaciers, Canada. Geophysical Research Letters 34, L16503. doi:10.1029/2007GL030780.

Shea, J.M., Moore, R.D., Stahl, K., 2009. Derivation of melt factors from glacier mass-balance records in western Canada. Journal of Glaciology 55 (189), 123–130.

Stahl, K., Moore, R.D., 2006. Influence of watershed glacier coverage on summer streamflow in British Columbia, Canada. Water Resources Research 42, W06201. doi:10.1029/2006WR005022.

Stahl, K., Moore, R.D., Floyer, J.A., Asplin, M.G., McKendry, I.G., 2006. Comparison of approaches for spatial interpolation of daily air temperature in a large region with complex topography and highly variable station density. Agricultural and Forest Meteorology 193, 224–236.

VanLooy, J.A., Forster, R.R., 2008. Glacial changes of five southwest British Columbia icefields, Canada, mid-1980s to 1999. Journal of Glaciology 54, 469–478.

Van Beusekom, A.E., O'Neel, S.R., March, R.S., Sass, L.C., Cox, L.H., 2010. Re-analysis of Alaskan Benchmark Glacier Mass-Balance Data Using the Index Method. U.S. Geological Survey Scientific Investigations Report 2010-5247. U.S. Geological Survey, Reston, Virginia.

WGMS, 2008. Fluctuations of glaciers 2000–2005. In: Haeberli, W., Zemp, M., Kääb, A., Paul, F., Hoelzle, M. (Eds.), ICSU(FAGS)/IUGG(IACS)/UNEP/UNESCO/WMO, Volume IX. World Glacier Monitoring Service, Zurich, Switzerland.